

CAAP Quarterly Report

12/30/2023

Project Name: Easy Deployed Distributed Acoustic Sensing System for Remotely Assessing Potential and Existing Risks to Pipeline Integrity

Contract Number: 693JK3215002CAAP

Prime University: Colorado School of Mines

Prepared By: Yilin Fan, yilinfan@mines.edu, 303-273-3749;
Ge Jin, gjin@mines.edu, 303-273-3455;
Ali Tura, alitura@mines.edu, 303-273-3454;
Jennifer Miskimins, jmiskimi@mines.edu, 303-384-2607

Reporting Period: [10/01/2023 – 12/30/2023]

Project Activities for Reporting Period:

During this period, we have made noticeable progress on the remaining tasks (Tasks#2, #3, #4, #6), which are discussed in the following. All the plots are shown at the very end.

Task#2. Detection of Dynamic Intermittent (Slug) Structure

In Task#2, we focused on detecting dynamic intermittent (slug) structures, and the following activities were undertaken:

- Modified the LabView program to enable the pressure recording frequency up to 10Hz, which better monitored the pressure fluctuations induced by slug flow.
- Repeated the experiments for 0.6 GPM under slug flow conditions at superficial gas velocity of 2, 4, and 6 m/s, with the new pressure recording frequency.
- Completed the experiments at another liquid flow rate (0.3 GPM) at various superficial gas velocities (18, 14, 10, 8, 6, 4, 2 m/s). The flow pattern is stratified flow (gas and liquid flow stably and separately) when the superficial gas velocity is greater or equal to 8 m/s, and slug flow (gas and liquid flow intermittently) for superficial velocities below or equal to 6 m/s. Figure 1 illustrates the schematic of the facility and fiber cable connections.
- Data processing was conducted which is discussed below along with the results.

The utilization of standard-deviated processed DAS data allows for accurately identifying slugs within a large time period. Figures 2-4 show the processed DAS data for 6, 4, and 2 superficial gas velocities at 0.6 GPM liquid flow rate, and Figures 5-7 show the processed data for 0.3 GPM liquid flow rate. Within the processed DAS data windows representing thin, flat, and thick cable sections, the distinctive sloping shape provided a visual trajectory of slugs over time. Additionally, the pressure sensor served as a supplementary monitoring method, enabling the comparison of processed DAS data at specific locations (36 m, 98.3 m, 132.3 m for thin, flat, and thick cable sections, respectively). The pressure measurement demonstrates the slug flow induced pressure fluctuations. The peaks denote when slugs are passing by, which are captured well by DAS. DAS can also distinguish the flow pattern very well. Figure 8 shows the signals for stratified flow, for

which the gas and liquid are flowing separately and stably, with minimal pressure fluctuations. On the other hand, the slug flow demonstrates intermittent flow behavior as illustrated in Figures 2-7.

Task#3. Detection of Corroded Spots on Pipeline Interior Surface

Throughout this reporting period, we successfully completed testing on the severely corroded 1-meter pipe featuring a minor leaking spot (Figure 9). Our experiments involved testing at five different flow rates (2, 6, 10, 14, 18 m/s) to comprehensively assess its behavior. The tests were conducted under two conditions: densely supported (6 supports) and sparsely supported (5 supports). We compared the recorded data with that of the control group in the leakage task (Task 6). To enhance detectability of the internal cables, the leak in the corroded pipe was strategically positioned at the bottom.

The previous setup involved the 1-meter pipe test section being connected to the entire steel pipe using fixed couplings, which we have replaced with hammer unions. Figure 10 shows the new setup. These new connections offer increased flexibility and ease of use. Their implementation facilitates the change of the 1-meter central pipe, significantly reducing the need for resplicing the fiber optics.

Preliminary data analysis indicates no clear leakage signals can be identified using the internal cables. However, the external straight cable exhibits increased vibration levels in the middle section, potentially correlating with the leak. This vibration could also stem from imperfect coupling between the straight fiber and the 1-meter section due to joint presence. The absence of a leakage-induced signal is likely due to the small size of the leak (2-3 mm), significantly smaller than those tested in Task 6. Additionally, the valve at the pipe's end was left open, causing only minor flow diversion into the leak and resulting in negligible vibrations undetectable by the internal cables.

Corrosion has reduced the material in the pipe section, leading to a thinner wall and lighter weight of the 1-meter section, potentially altering the entire pipe's resonant frequencies. Figure 11 presents a spectrum comparison between the control test and the corroded case at a 10 m/s flow rate. Although the spectra recorded by different cables are consistent, the resonant frequencies differ significantly between the control and corroded tests. Notably, the change in even-number modes (with the largest amplitude in the pipe's middle section, where corrosion is prevalent) is more pronounced than in odd-number modes. This difference, however, is likely attributable to the hammer union joints' alteration of the pipe's elastic properties, rather than the corrosion itself. A control test incorporating hammer union connections will be conducted next quarter to establish a more comparable control group for identifying corrosion-related signal changes.

Additionally, within our lab facilities, we finalized the development of another 1-meter test section. This new section exhibits a corrosion depth of approximately 5.5 mm without any leakage. We were unable to complete the testing of this pipe due to the Edgar Mine's schedule resulting in it being closed for several weeks during the semester. We are planning to test it in the upcoming quarter.

Task#4. Detection of Dent/Deformation on Pipeline

During this reporting period, we completed the testing of two dented pipes prepared in the previous quarter (Figure 12). One pipe showcased a substantial deformation, simulating a significant structural compromise, while the other presented a smaller dent, simulating a less severe scenario. Figure 13 illustrates the facility with the dented pipeline positioned at the center of the steel pipe. We conducted experiments on both pipes, testing five different flow rates (2, 6, 10, 14, 18 m/s). The resulting data were compared to experiments conducted on the central 1-m section of the pipe without defects, serving as our baseline or control experiment in the data processing workflow section.

We conducted a Fourier spectrum analysis on the DAS measurements. For this task, this analysis aimed to qualitatively assess the vibrational modes of the pipe, comparing the dented pipes with the control experiment. This data processing workflow is similar to the one applied in Task#6.

In our analysis, raw DAS data were segmented into 10-second intervals, and amplitude spectra were computed for each channel. To enhance statistical reliability, spectra obtained from 4-minute measurements during the same experiments were stacked and averaged. These resulting spectra were organized into 2D arrays, where each column represented spectrum amplitude for a specific frequency, and each row corresponded to the amplitude spectrum for an individual channel. Figure 14 depicts the 2D spectra obtained from experiments involving large and small dents, respectively, compared to the baseline experiment.

To further comprehend the dataset, we calculated pipe vibration frequencies measured by different cables. Figure 15 and Figure 16 present the vibration frequencies for large and small dents, respectively. An intriguing observation was the shift in frequencies for only even-indexed modes (indicated by black dashed lines) between the dent (orange line) and control (blue line), while odd-indexed modes (red dashed lines) did not exhibit a frequency shift. This phenomenon can be explained by the fact that even modes display the highest amplitude at the pipe center, making them more sensitive to structural changes there, whereas odd modes possess zero amplitude at the pipe center, rendering them insensitive to the dent presence at the center of the pipe.

Moving forward, our upcoming efforts will focus on conducting additional analysis and refining our workflow to delve deeper into comprehending the underlying physics behind our findings and ensuring their reliability. This progress will be detailed in the next report to be submitted.

Task#6. Detection of Leakage

In this reporting period, we conducted repeated leakage experiments to enhance the reliability of our findings. We successfully reproduced the results and improved upon some of them. Same as reported previously, the leakage tests involved a 1-m test section featuring 1" holes positioned at three different orientations to simulate various leakage scenarios. Through the use of reducers, we were able to test four different leakage sizes: $\frac{1}{4}$ ", $\frac{1}{2}$ ", $\frac{3}{4}$ ", and 1". Additionally, we conducted tests using five gas flow rates: 2, 6, 10, 14, and 18 m/s. Prior to each leakage experiment, a control experiment (without any leakage) was conducted to ensure a more consistent basis for comparison.

In this section, we'll briefly review the data processing workflow outlined in our previous quarterly report, which we've consistently applied to process the data collected during this reporting period.

The DAS data were recorded at a frequency of approximately 5600 Hz along a 480-meter fiber, generating a substantial volume of data in a short period. For instance, the three-hour recording session yielded over 150 GB of DAS data. Due to its size, this data set requires pre-processing before any meaningful analysis can be conducted. The first processing we conducted was based on the standard deviation (STD). We segment the data set into one-second intervals and compute the STD for each channel within each second. These STD values are then concatenated into a continuous data set with a 1 Hz sampling rate. This method allows for a data reduction factor of 5600, equivalent to the original sampling rate. Figure 17 provides an illustrative example of the STD data attributes during an experiment involving bottom leakage holes. In this figure, a higher value (depicted in red) signifies a larger standard deviation at a specific time and location along the sensing fiber, which in turn is indicative of higher vibration intensity experienced by the cable section.

The figure displays the vibration intensity for four distinct types of cables during the experiment conducted on the same day. The study commenced with a control experiment featuring no leakage, followed by the sequential introduction of 1", ¾", ½", and ¼" leakage holes at the bottom of the test pipe. For each hole size, flow rates of 2, 6, 10, 14, and 18 m/s were examined. Figure 17 clearly reveals variations in fiber vibration intensity at different flow rates, with higher flow rates inducing stronger vibrations across all cable types.

Notably, more intense vibrations are visible near the pipe's center, where the leakage was introduced, for straight, black, and flat cables. The vibration anomaly appears to diminish with decreasing hole size and is entirely absent in the control tests.

Unlike the experimental setup detailed in the previous quarterly report, this time, the straight cable was secured to the pipe using duct tape, significantly improving the mechanical coupling of the fiber. This enhancement notably increased the cable's detectability, this can be seen clearly from the standard deviation data.

To quantify the vibration anomalies associated with the leakage points, we calculated the average vibration intensity over a four-minute span in the middle of each experiment. This average intensity forms a vibration profile for each cable, and the amplitude is then converted to decibels (dB) for easier comparison.

Figure 18 illustrates the sensitivity of various cables to different leakage sizes, particularly at a flow rate of 10 m/s. The thick cable, being notably heavier, shows the least sensitivity to vibrations induced by the leakage. However, the other three cable types demonstrate varying degrees of sensitivity to detect the vibration anomaly caused by different leakage sizes. It's noteworthy that improving the mechanical coupling of the straight cable significantly contributed to enhancing its ability to detect the vibration anomaly caused by leakage, as depicted in Figure 18.

Leakage detection sensitivity is also influenced by the gas flow rate within the pipe. Figure 19 illustrates the vibration distribution along the four fiber cables at different flow rates. For instance, in the control experiment, vibration intensity escalates with increasing flow rates for the flat cable, and no vibration anomaly is observable at the pipe's center. Conversely, in the experiment with a

½" leakage hole, a vibration anomaly is observable at all flow rates for straight, flat, and black cables, while the thick cable shows no such response.

Our findings indicate that black and flat internal cables provide the most reliable leakage detection results observed thus far. Their lighter and more flexible structures likely increase their sensitivity to fluid movements within the pipe. Furthermore, it's worth noting the validation of our hypothesis: improving the mechanical coupling between the external cable and the steel pipe notably enhanced its detectability.

To better understand the cable vibrations induced by leakage, we conducted a Fourier spectrum analysis on the DAS measurements. The primary objective of this analysis is to identify the frequency range associated with the leakage-related signals. Acquiring this information will aid in optimizing leakage detection algorithms and refining future data acquisition parameters.

The resulting spectra are organized as 2D arrays, where each column represents the spectrum amplitude for a specific frequency and each row corresponds to the amplitude spectrum for an individual channel.

Figure 20 illustrates the 2-D spectra obtained from experiments involving various leakage sizes at the bottom of a pipe with a flow rate of 10 m/s. High amplitude spectra are conspicuously evident near the leakage points (indicated by blue arrows in Figure 20) for most cases involving straight, black and flat cables. However, the leakage point is less identifiable in the spectra of thicker cables.

To visualize the amplitude spectrum induced by the leakage more clearly, we extracted the amplitude values corresponding to the leakage location from the 2D spectra and plotted them against frequency. Figure 21 presents the amplitude spectrum for experiments with different leakage sizes, all at a flow rate of 10 m/s. The right column of Figure 21 shows the amplitude ratio between the leakage and control (no leakage) experiments. Our findings indicate that the vibrational anomalies caused by leakage span a broad spectrum. For black cable, we observed up to a 10 dB increase in amplitude across most of the measured frequency range at the leakage point compared to the no-leakage scenario.

The spectral responses appear to be more complex for flat cable. For instance, with leakage sizes of ¼" and ¾", amplitude increases are more uniformly distributed across the entire frequency band, averaging between 1-2 dB. Conversely, for ½" and 1" leakage sizes, the amplitude increases are predominantly concentrated in the 1000-2000 Hz range, exceeding an average of 5 dB. This complex response to leakage is likely due to the flow interactions between the flat cable and the flow deviating from the main pipe into the leakage pathway. Similarly, the straight cable exhibits an amplitude increase concentrated in the same frequency range (1000-2000Hz range). In contrast, little amplitude increase can be observed on the thick cable, which is consistent with the STD results. At large leakage sizes, amplitude increase can be observed at a narrower frequency band, with 600-800 Hz for the ¾" leakage size and 1100-1300 Hz for the 1" leakage size.

From the results, we found that the black cable seems to provide more reliable differentiation between leakage and control experiments, which could potentially lead to more reliable leakage detection.

Project Financial Activities Incurred during the Reporting Period:

The following table summarizes the financial activities and the corresponding expenses during the reporting period. Also shown are the budget for the third year and the total expenses so far. Please note that the actual amount for the expenses might be slightly different from the numbers in the final financial report, since some of the expenses occurring in late of the quarter may not be included in the university’s financial system that we use for managing the funds and expenses by the time the report is submitted. Normally, it takes several days for an expense to be shown in the system after its occurrence.

Items\Budget and Expenses		Total Budget for Year 3	Total Expenses in Year 3	Expenses During Reporting Period
1	Faculty Salaries and Wages including Fringe Benefits	\$29,471	\$0	\$0
2	Student Salaries	\$33,949	\$17,884	\$17,884
3	Graduate Student Tuition	\$47,186	\$0	\$0
4	Experimental Expenses (experimental work supplies, services, maintenance, cables, etc.)	\$27,000	\$1672	\$1672
5	Travel	\$3,000	\$0	\$0
6	Indirect Costs (51.5%)	\$48,578	\$10,071	\$10,071
Total		\$235,392	\$29,627	\$29,627

Project Activities with Cost Share Partners:

The cost shares are the AY efforts of the PI and co-PIs. Activities are the same as above.

Project Activities with External Partners:

No external partners.

Potential Project Risks:

Same as the previous reports. The most influential factors that can potentially delay the project progress in this coming quarter are the snowy weather, Edgar Mine’s operating schedule, and students’ course/exam schedule, which limit the days the students can work at the Edgar Mine. The team is trying the best to keep the progress on track, but please note that there are still risks of delay because of the factors mentioned above.

Future Project Work:

In the next 30 days, we will:

1. Repeat some of the tests in Task#3 for supported pipes and conduct some additional ones as needed such as the control test.
2. Start the experiments in Task#3 for unburied pipe.

In the next 60-90 days, we will:

1. In addition to the previous tasks, start the experiments for buried pipe.

Potential Impacts to Pipeline Safety:

Tasks#1 and #2 can potentially help identify and characterize the possible liquid accumulation in a gas gathering or transmission pipeline using DAS, while Tasks#3-6 will potentially help detect the internally corroded surface, deformation, infrastructure damage, and leakage in a gas pipeline.

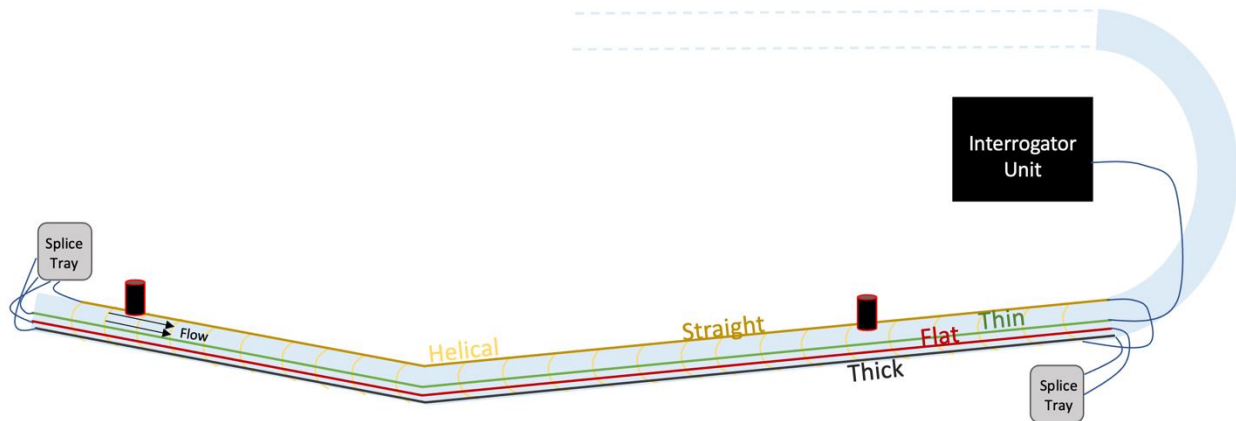


Figure 1. Schematic of Task #2 Layout depicting the interrogator unit spliced to a sequence of cables, including thin, flat, thick, straight, and helical sections. Two sensors are strategically positioned both uphill and downhill along the experimental segment of the flow loop. Notably, the pressure sensor situated on the downstream section was replaced with a higher frequency sensor.

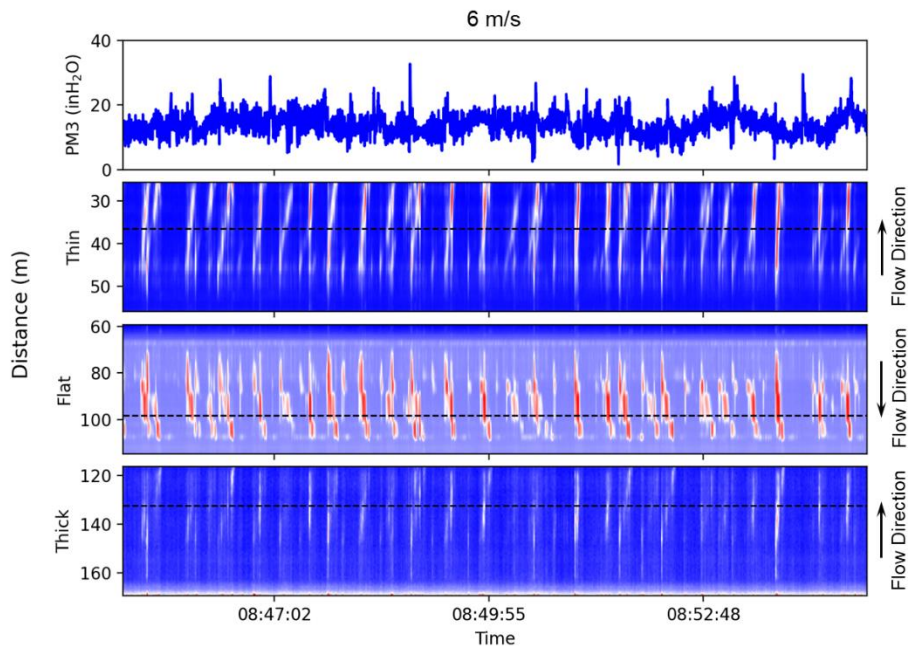


Figure 2. Processed standard deviation DAS data depicting the thin, flat, and thick cable sections, co-plotted with pressure sensor data (top). The black dashed lines on the thin, flat, and thick sections denote the position of the pressure sensor within each cable section. The observed slugging behavior is illustrated by slight, sloping trends in varying directions for each cable, indicating the slug's location at different times. The flow direction is also indicated by the black arrow on the right. The current superficial gas velocity is 6 m/s, and the liquid flow rate is 0.6 GPM (superficial liquid velocity is around 0.005 m/s).

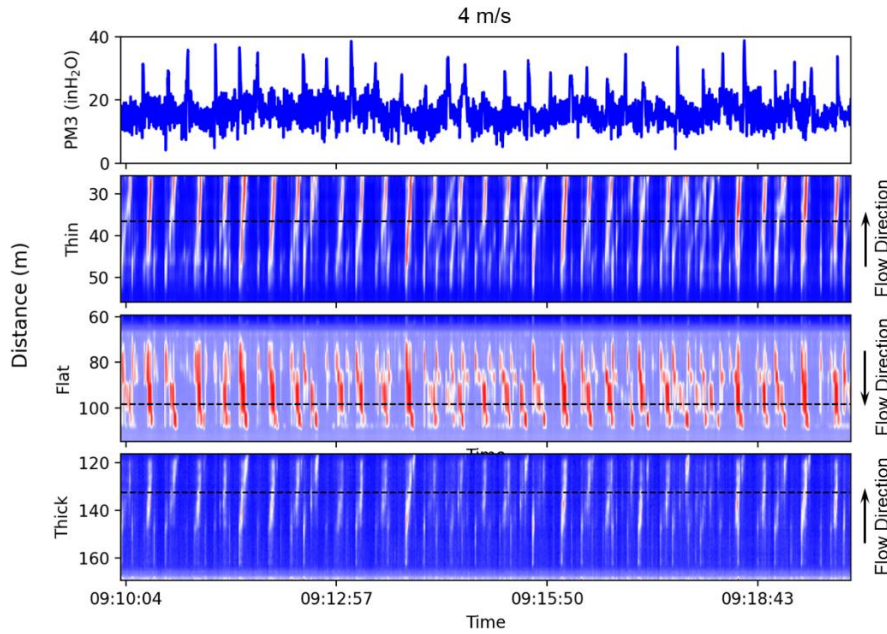


Figure 3. Processed standard deviation DAS data depicting the thin, flat, and thick cable sections, co-plotted with pressure sensor data (top). The black dashed lines on the thin, flat, and thick sections denote the position of the pressure sensor within each cable section. The observed slugging behavior is illustrated by slight, sloping trends in varying directions for each cable, indicating the slug's location at different times. The flow direction is also indicated by the black arrow on the right. The current superficial gas velocity is 4 m/s, and the liquid flow rate is 0.6 GPM (superficial liquid velocity is around 0.005 m/s).

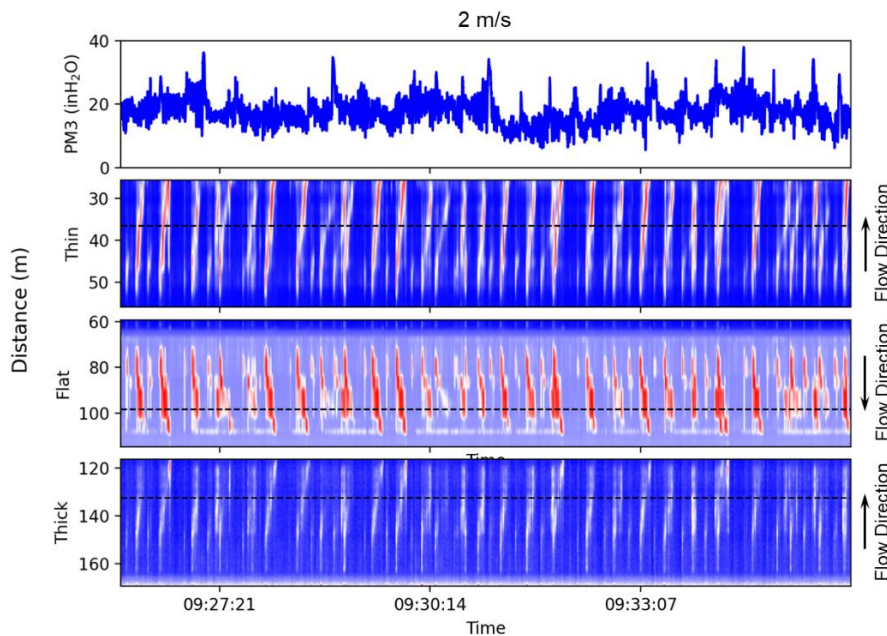


Figure 4. Processed standard deviation DAS data depicting the thin, flat, and thick cable sections, co-plotted with pressure sensor data (top). The black dashed lines on the thin, flat, and thick sections denote the position of the pressure sensor within each cable section. The observed

slugging behavior is illustrated by slight, sloping trends in varying directions for each cable, indicating the slug's location at different times. The flow direction is also indicated by the black arrow on the right. The current superficial gas velocity is 2 m/s, and the liquid flow rate is 0.6 GPM (superficial liquid velocity is around 0.005 m/s).

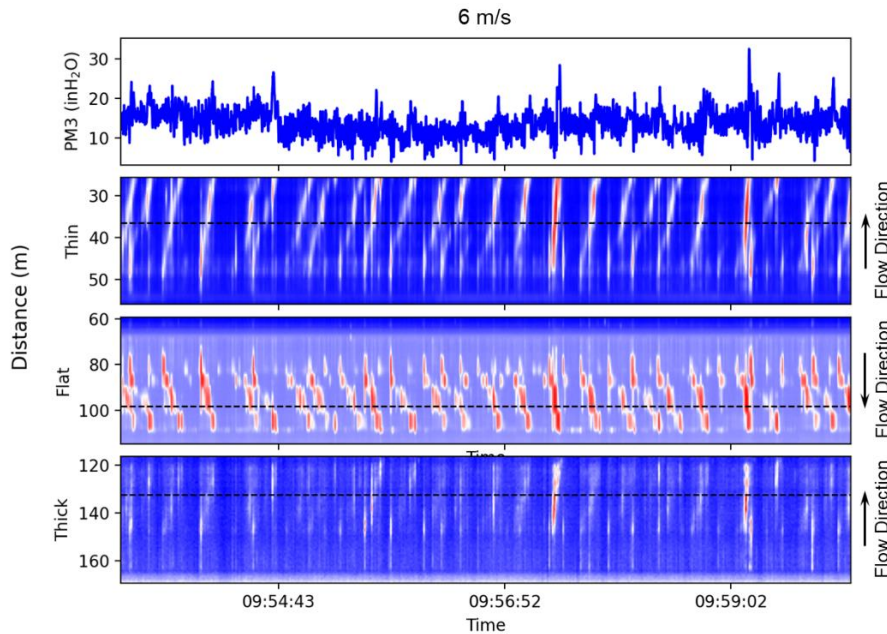


Figure 5. Processed standard deviation DAS data depicting the thin, flat, and thick cable sections, co-plotted with pressure sensor data (top). The black dashed lines on the thin, flat, and thick sections denote the position of the pressure sensor within each cable section. The observed slugging behavior is illustrated by slight, sloping trends in varying directions for each cable, indicating the slug's location at different times. The flow direction is also indicated by the black arrow on the right. The current superficial gas velocity is 6 m/s, and the liquid flow rate is 0.3 GPM (superficial liquid velocity is around 0.0025 m/s).

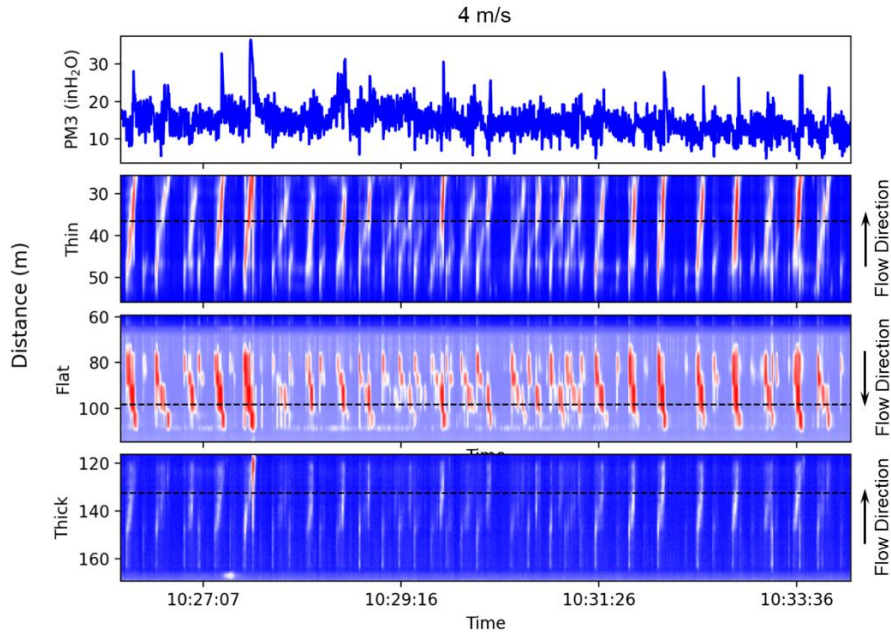


Figure 6. Processed standard deviation DAS data depicting the thin, flat, and thick cable sections, co-plotted with pressure sensor data (top). The black dashed lines on the thin, flat, and thick sections denote the position of the pressure sensor within each cable section. The observed slugging behavior is illustrated by slight, sloping trends in varying directions for each cable, indicating the slug's location at different times. The flow direction is also indicated by the black arrow on the right. The current superficial gas velocity is 4 m/s, and the liquid flow rate is 0.3 GPM (superficial liquid velocity is around 0.0025 m/s).

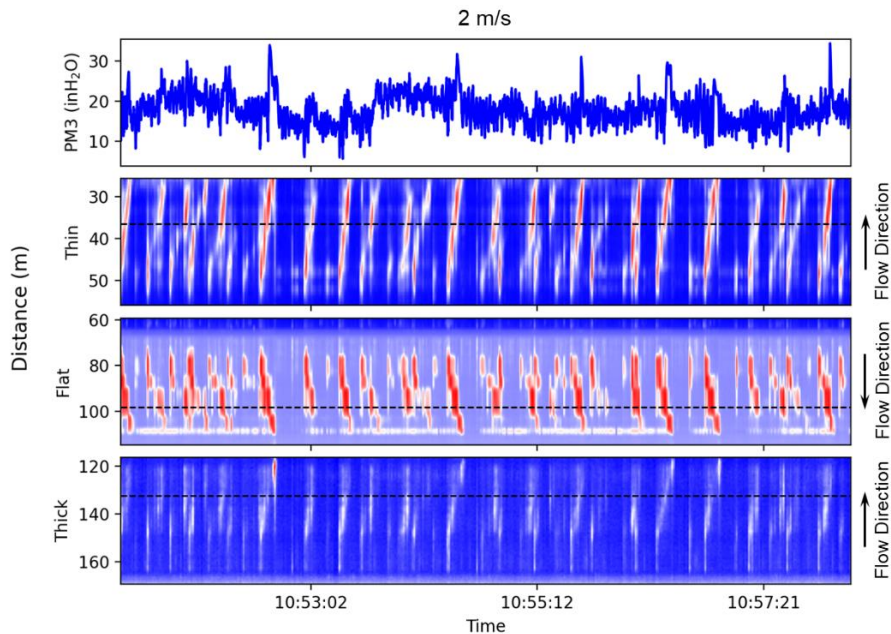


Figure 7. Processed standard deviation DAS data depicting the thin, flat, and thick cable sections, co-plotted with pressure sensor data (top). The black dashed lines on the thin, flat, and thick sections denote the position of the pressure sensor within each cable section. The observed

slugging behavior is illustrated by slight, sloping trends in varying directions for each cable, indicating the slug's location at different times. The flow direction is also indicated by the black arrow on the right. The current superficial gas velocity is 2 m/s, and the liquid flow rate is 0.3 GPM (superficial liquid velocity is around 0.0025 m/s).

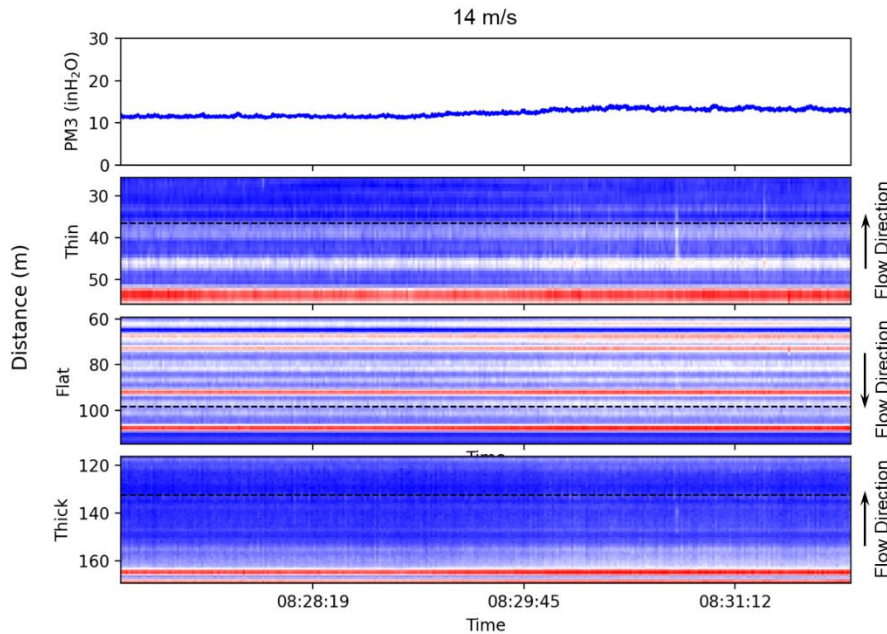


Figure 8. Processed standard deviation DAS data depicting the thin, flat, and thick cable sections, co-plotted with pressure sensor data (top). The black dashed lines on the thin, flat, and thick sections denote the position of the pressure sensor within each cable section. The flow direction is indicated by the black arrow on the right. The flow pattern is stratified flow. The signal does not vary much with time, indicating stable fluid flow behaviors as it should be in stratified flow. The current superficial gas velocity is 14 m/s, and the liquid flow rate is 0.3 GPM (superficial liquid velocity is around 0.0025 m/s).



Figure 9. Photograph of the 1-m corroded pipe with minor leakage (~2mm) at pipe bottom



Figure 10. photograph of the 1-m corroded pipe with the minor leakage connected to the steel pipe using hammer unions

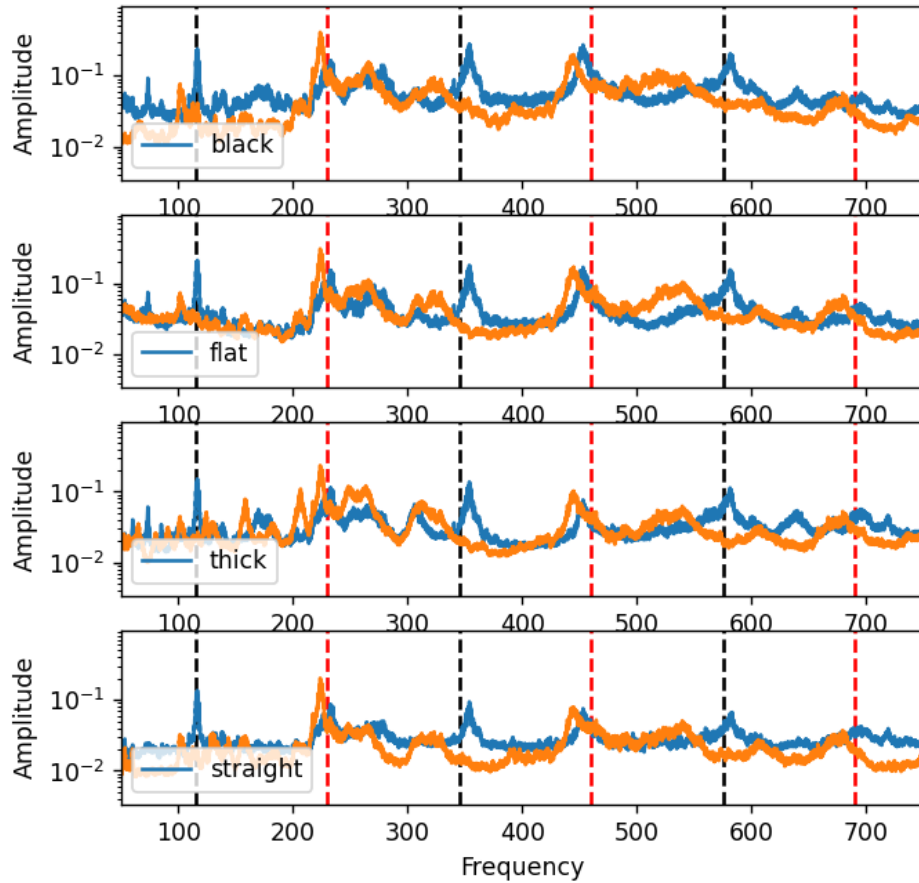


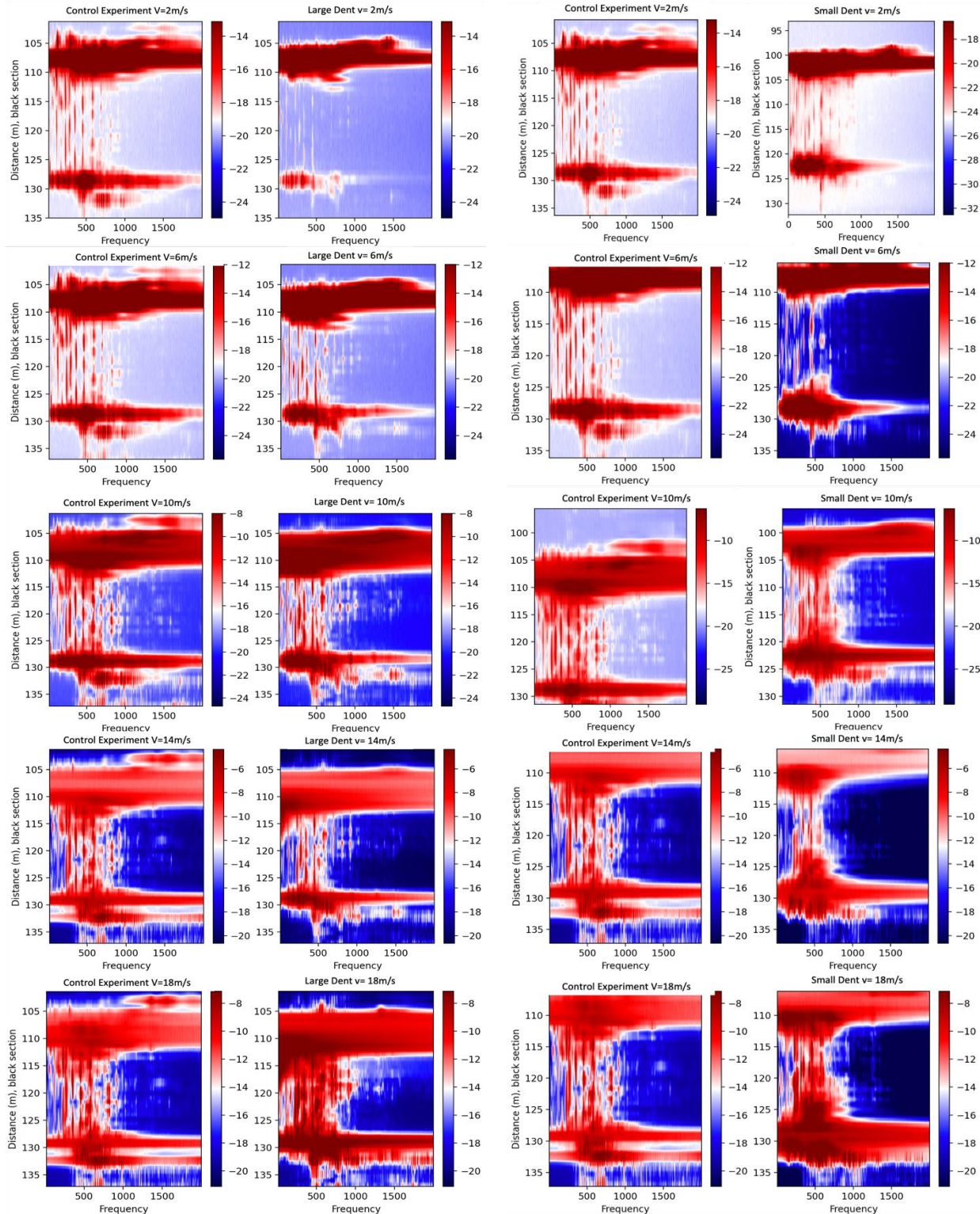
Figure 11. Pipe vibration spectrum recorded at different cables during control test (blue) and severe corroded pipe (orange). The gas flow rate is 10 m/s. Black dashed lines show even number modes while the red dashed lines show odd number modes.



Figure 12. Photograph of the facility that created the dents and the 1-m test sections with two dent sizes.



Figure 13. Photograph of the 1-m pipe with large dent positioned at the center of the steel pipe



(a) Large dent

(b) small dent

Figure 14. 2D spectra of black cable section with varying flow rates for large dented (a) and small dented (b) pipes.

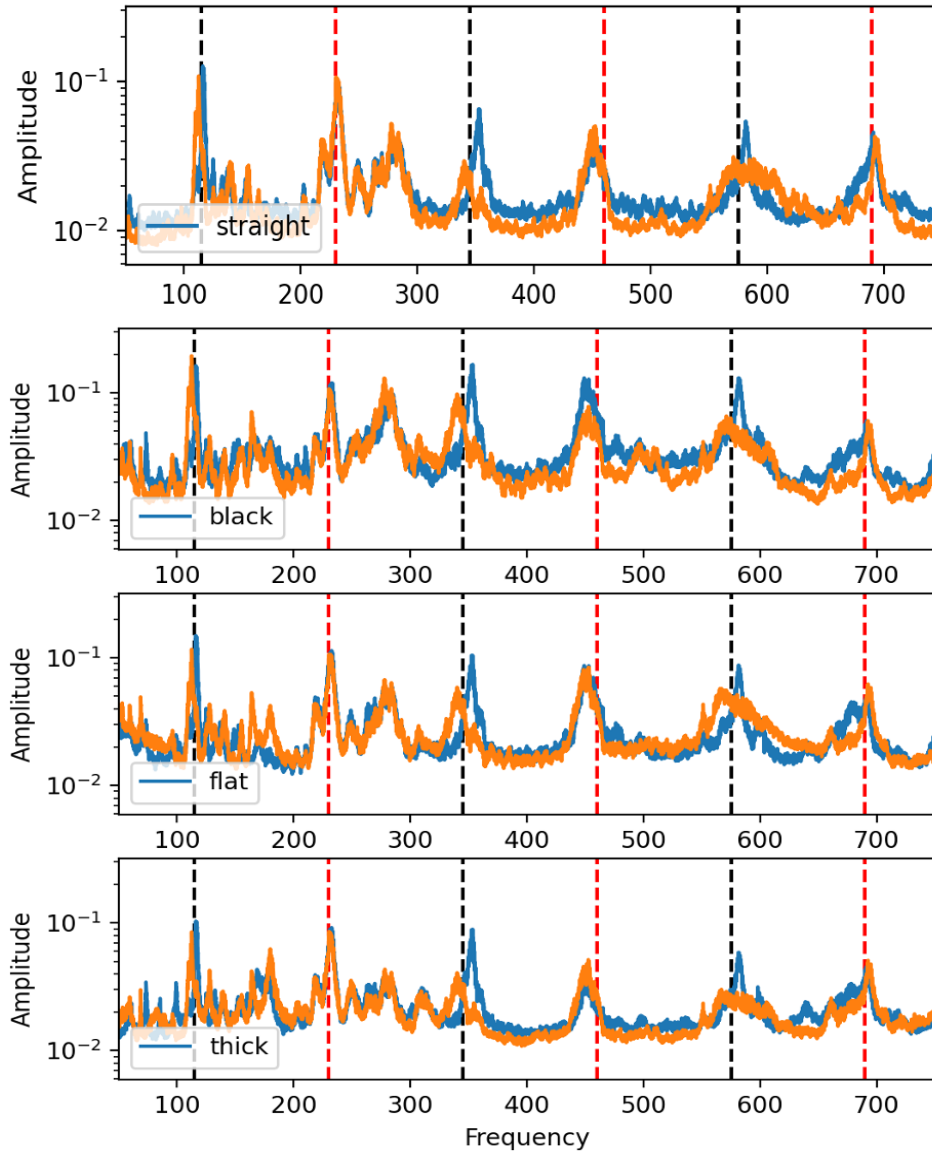


Figure 15: Vibration frequencies measured by different cables (large dent). Orange line presents data from the dented pipe while Blue line is data from the control experiment

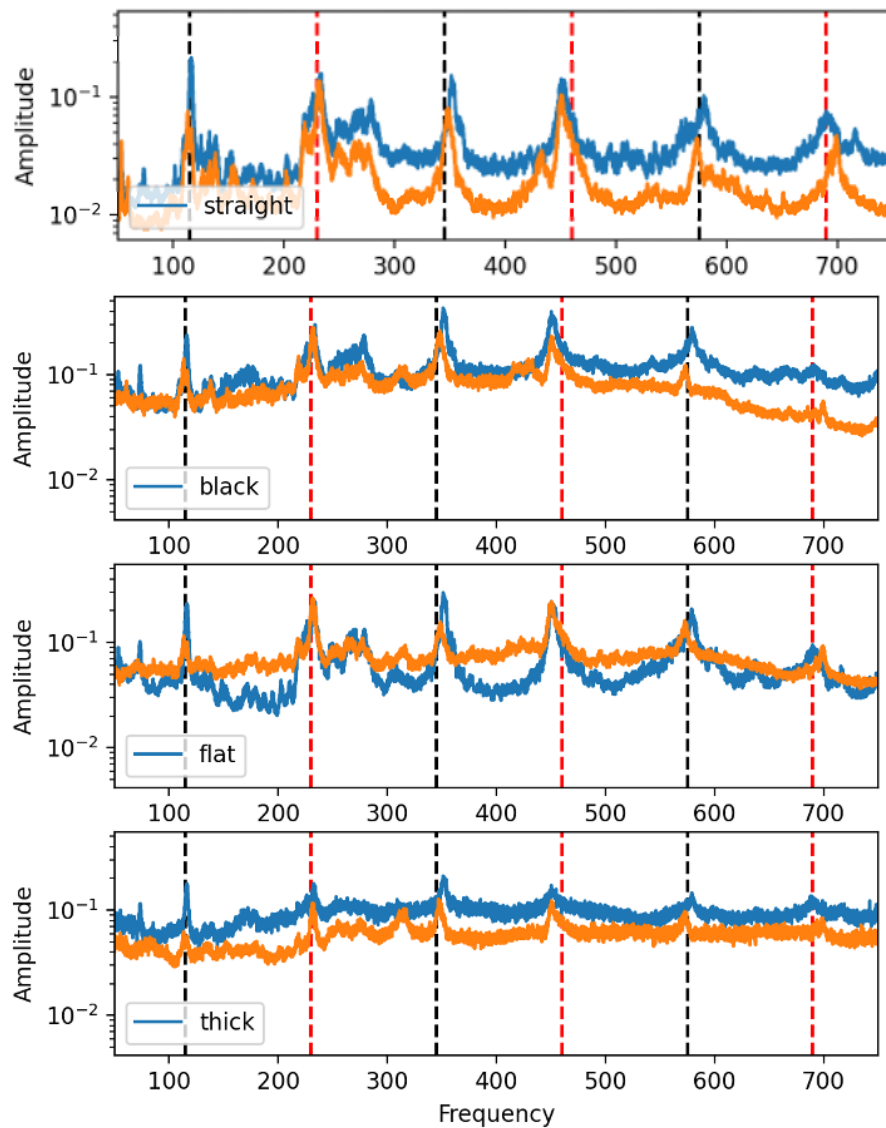


Figure 16: Vibration frequencies measured by different cables (large dent). Orange line presents data from the dented pipe while Blue line is data from the control experiment

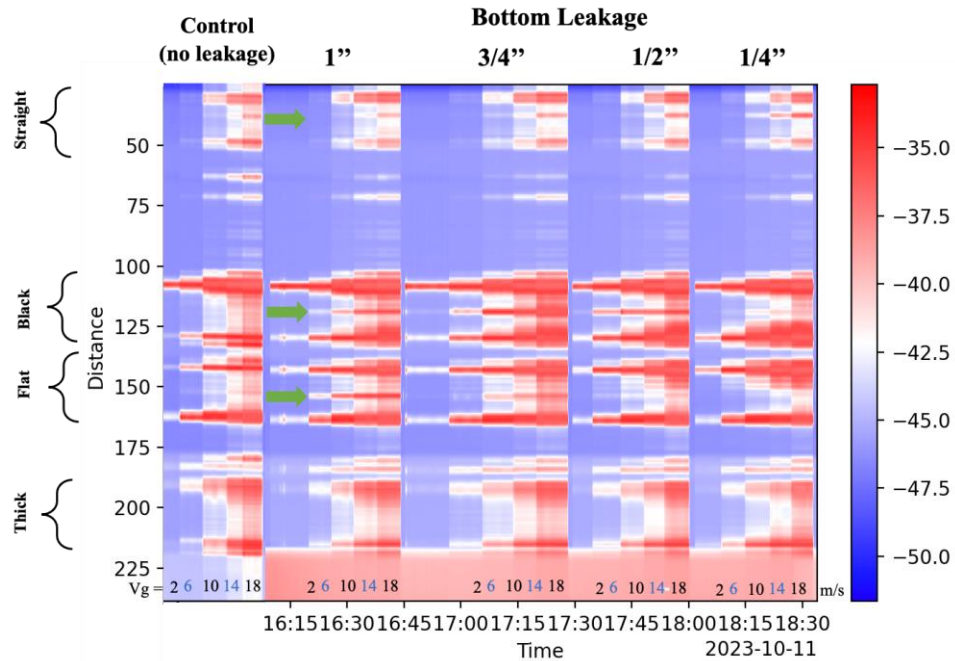


Figure 17. Magnitude of standard deviation values along the fiber during the experiment on October 11th, 2023. For each hole size, the flow rate changes from 2, 6, 10, 14 and 18 m/s. The gas velocities are indicated at the bottom of the image.

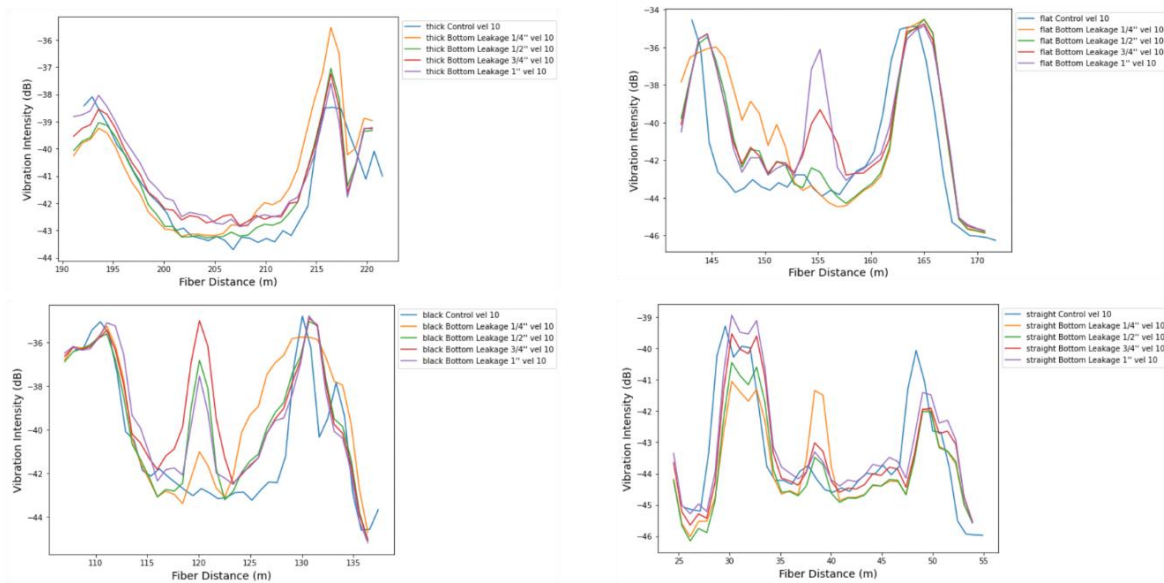


Figure 18. vibration intensity profiles in thick (upper left), flat (upper right), black (bottom left), and straight (bottom right) fiber sections during the leakage experiment. The different curves represent vibration intensities associated with varying leakage hole sizes at a flow rate of 10 m/s. Anomalies in vibration, induced by leakage holes and marked by blue arrows, are observable in three cable types when the hole size exceeds 1/2 inch.

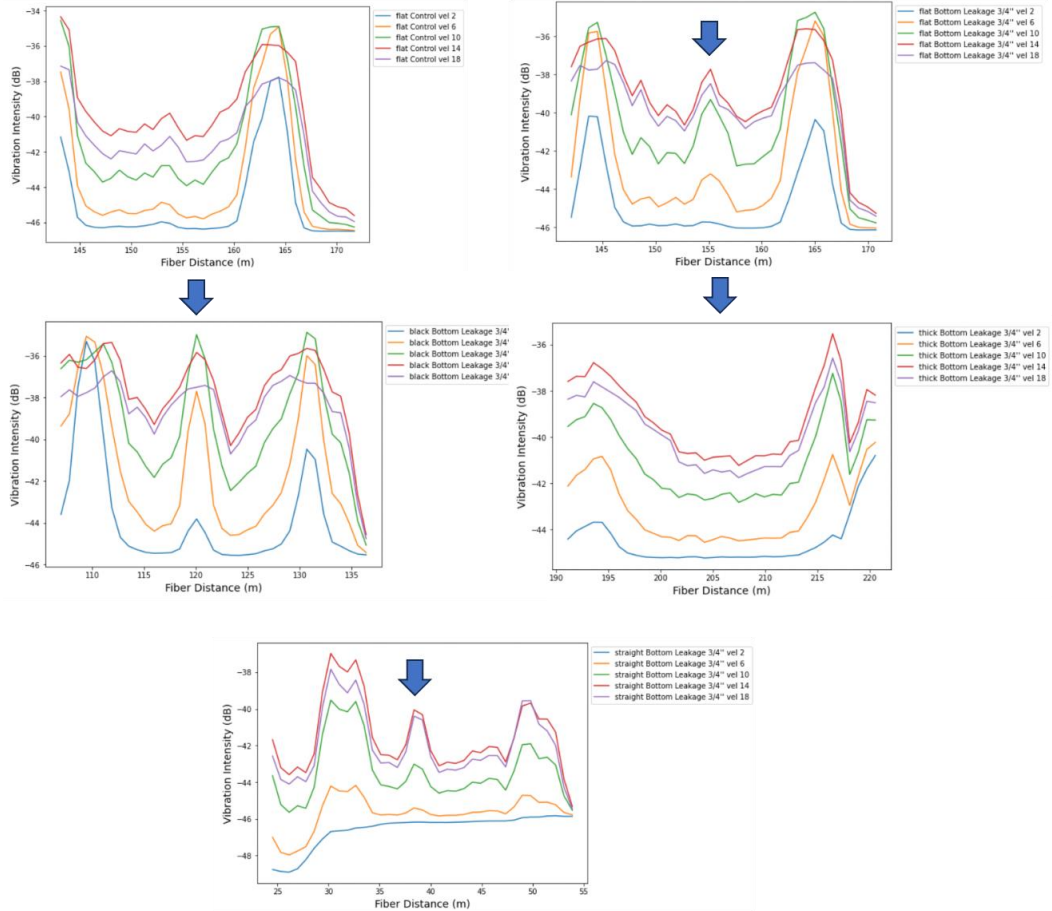


Figure 19. This figure compares the leakage detection sensitivity across different cable types at varying flow velocities. Top left shows a flat cable without leakage as a control experiment. Top right features a flat cable with a leakage hole size of 3/4 inch. The middle left, middle right, and bottom sections present the black, thick, and straight cables with the same leakage size, respectively.

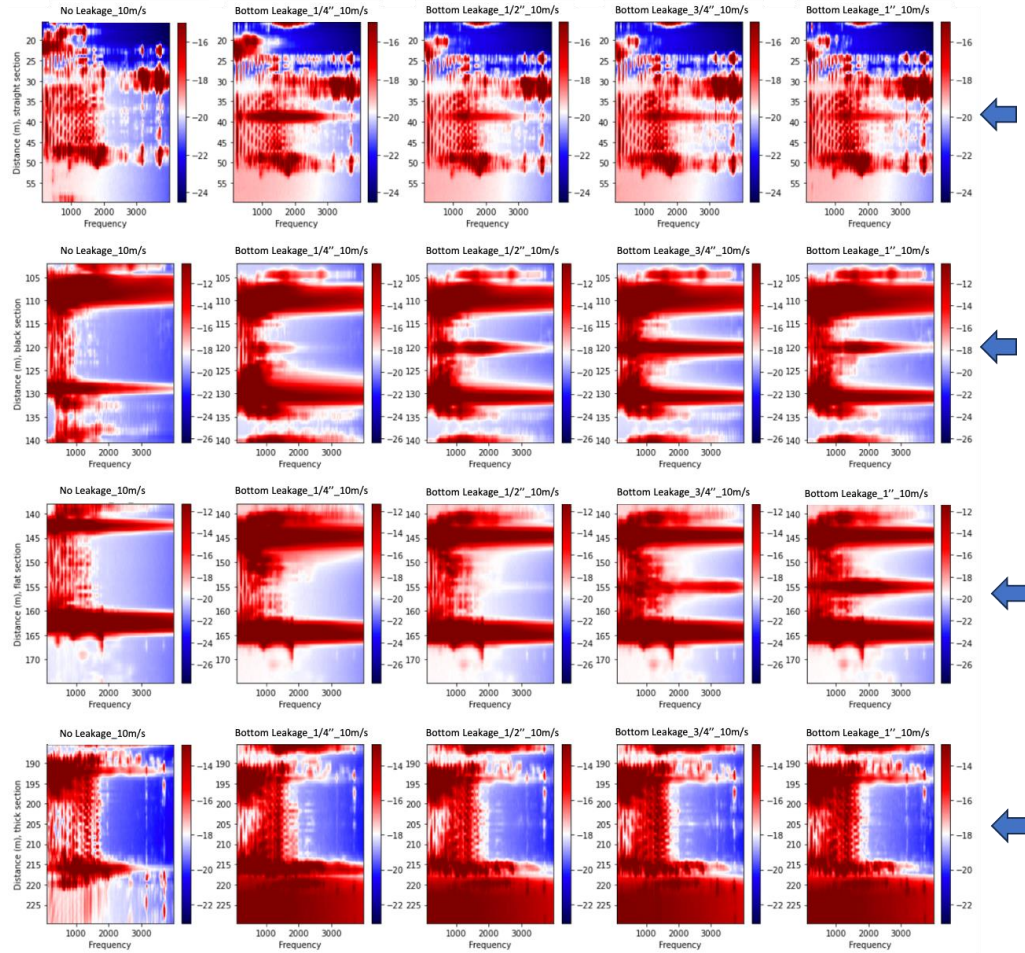


Figure 20. 2D spectra of fiber sections with varying leakage hole sizes at the bottom of the pipe, measured at a flow rate of 10 m/s. The top row displays the straight cable section, followed by the black, the flat, and the thick cable sections. Columns from left to right represent the control experiment (no leakage), followed by leakage sizes of 1/4", 1/2", 3/4", and 1", respectively. The color scale is measured in dB. Blue arrows show the leakage point location.

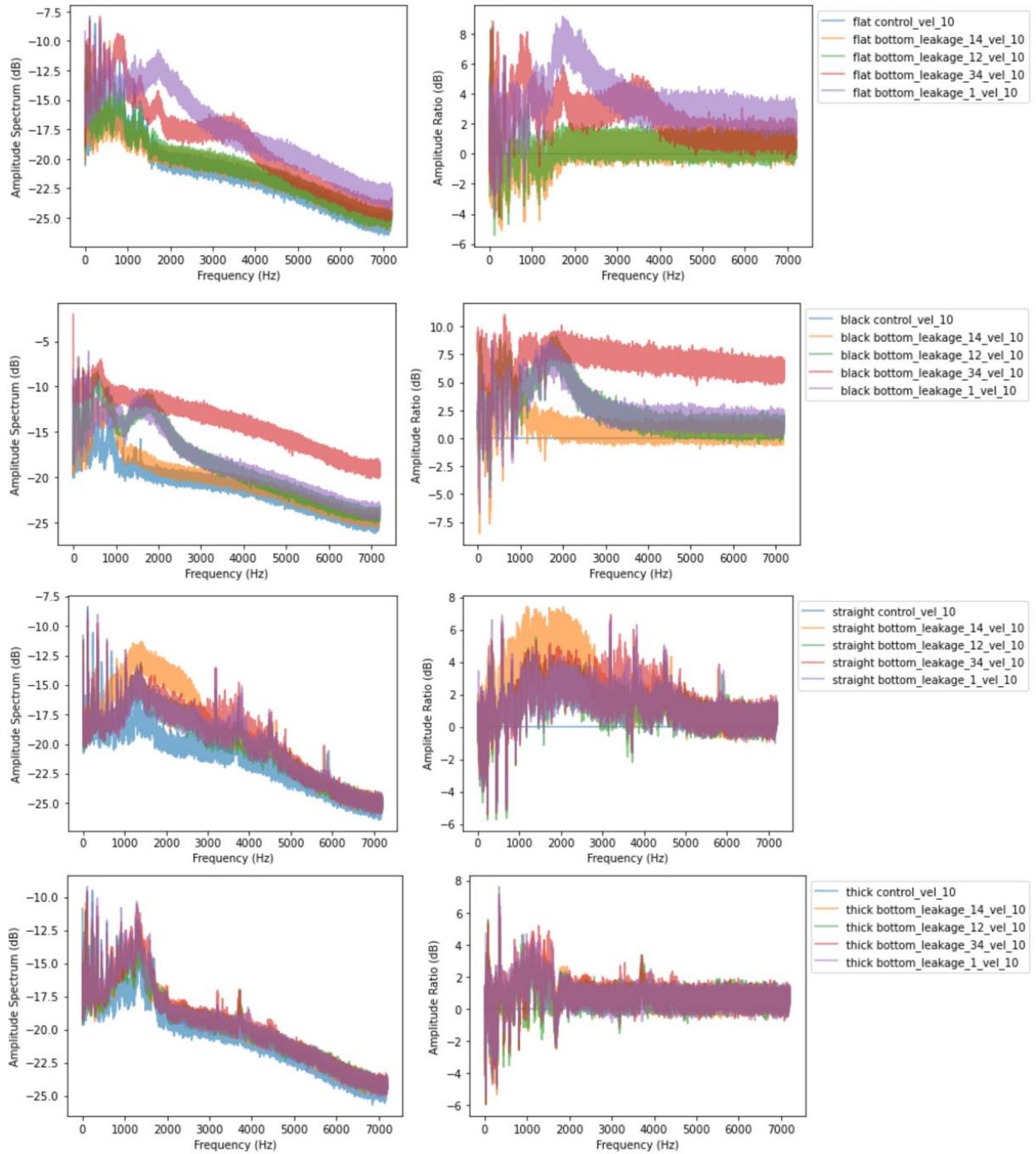


Figure 21. Amplitude spectrum at leakage point locations for various cables and leakage sizes. The flow rate is 10 m/s. The first row displays results for flat cable, the second row for black cable, the third row for the straight cable, and the fourth row for thick cable. The left column shows the amplitude spectrum, while the right column presents the ratio of amplitude spectrum between leakage experiments and the control experiment. All values are expressed in decibels (dB).